Supplementary Materials for

# Anionic Redox Reaction Triggered by trivalent $Al^{3+}$ in P3-$Na_{0.65}Mn_{0.5}Al_{0.5}O_2$

The file includes:

**Acknowledgments**

**Experimental Section**

**Figure S1 to S9**

**Tables S1 to S3**

**References**

**Acknowledgments**

This work was financially supported by the NSAF (Grant No. 1921773037 and U20A20336), the National Key Scientific Research Project (Grant No. 2016YFB090150), and Tianmu Lake Institute of Advanced Energy Storage Technologies Scientist Studio Program [No. TIES-SS0002]. The work at Brookhaven National Laboratory was supported by the U.S. Department of Energy, the Assistant Secretary for Energy Efficiency and Renewable Energy, Vehicle Technology Office through Advanced Battery Material Research (BMR) program under Contract No. DE-SC0012704. This research used resources at beamlines 7-BM (QAS) and 23-ID-2 (IOS) of the National Synchrotron Light Source II, a U.S. Department of Energy (DOE) Office of Science User Facility operated for the DOE Office of Science by Brookhaven National Laboratory under Contract No. DE-SC0012704.

## Experimental Section

**Material preparation:** The precursor $MnAlO_x$ (MAO) were prepared by the co-precipitation method. 0.01M $AlCl_3 \cdot 6H_2O$ (SCR Co., Ltd, 97%) and 0.01 M $MnCl_2$(XINGTA, 99%) were dissolved in 100 ml water, 0.75 M $Na_2CO_3$ (50% excess) were then slowly added into the solution with continuous stirring. The obtained precipitate $MnAlO_m(OH)n$ were washed with distilled water and then dried in a blowing oven at 80°C. Precipitate $MnAlO_m(OH)n$ were calcined at 350°C for 6h to obtain the processor $MnAlO_x$ (MAO). Samples of $Na_{0.65}Al_{0.5}Mn_{0.5}O_2$ were prepared by solid-state reactions of stoichiometric amounts of $Na_2CO_3$ (Alfa Aesar, 98%) and processor $MnAlO_x$ (MAO). The starting powders were ball-milled for 6h and then pressed into a pellet. The pellet was heated at 900°C for 12 hours in $O_2$ phenomena. After a cooling process, the resulting product was transformed into Ar-filled glove box immediately to avoid contact with moisture.

**STEM measurement:** The STEM high-angle annular-dark-field (HAADF) and were obtained by a field-emission transmission electron microscope (JEOL ARM200F, 200 keV) operated at 200 kV and equipped with a Cs corrector (CEOS GmbH, Heidelberg, Germany).

**Electrochemical characterization:** Electrodes were prepared by a dry coating method in a glove box. The mixture of 80 wt% active material, 10 wt% Super P conductive carbon, and 10 wt% polytetrafluoroethylene (PTFE) binder was grounded hardly in a mortar, rolled to thin free-standing films. Electrochemical testing was carried out in 2032 coin cells with a Na metal-disk as the anode, glass fiber (Whatman GF/F) as the separator, and 1 M $NaClO_4$ dissolved in ethylene carbonate (EC)/propylene carbonate (PC) (1:1 in volume) as the electrolyte. Galvanostatic charge-discharge experiments were carried out on a Land CT2001A battery tester at room temperature. Cyclic voltammograms (CV) and AC impedance tests were performed on an electrochemical workstation CHI 660B.

**X-ray absorption spectroscopy:** XAS of Mn- K edge was measured at beamline 8-ID

and 7-BM of National Synchrotron Light Source II (NSLSI-II) in Brookhaven National Laboratory (BNL). The data were collected in the transmission mode. O K-edge XAS spectra were obtained in the fluorescence mode at beamline 23-ID-2 (IOS) of the NSLS-II in BNL. The X-ray absorption near-edge structure (XANES) spectra were processed using the Athena software package. [1]

**Ex-situ XRD measurements:** Ex-situ XRD patterns during the first cycle were collected on an X-ray diffractometer (Bruker D8 Advance, Germany) with Cu-Kα radiation (λ = 0.1540 nm) at 40 kV, 40 mA. In case of contact with air, samples were sealed in the sample holder with thin amorphous tape before removing from the Ar-filled glove box.

**XPS characterization**: XPS spectra were carried out on a PHI5300 System with a monochromatic Mg-$K_\alpha$ X-ray source at 250 W, 14 kV. The C 1s peak at 285.0 eV from hydrocarbon contamination was used to calibrate the bonding energy. The analysis of XPS data was performed using the XPS Peak Fitting Programme version 4.1.

**SEM and EDX:** Scanning electron microscope (SEM) images and Energy-dispersive X-ray spectroscope (EDX) were carried out by a field-emission scanning electron microscope (FE-SEM, Hitachi S-4800) operated at an acceleration voltage of 10 kV.

**Raman measurement:** Raman spectra were carried out by using Raman microscopes (Renishaw, UK) under 514-nm excitation.

**DFT+U calculations:** The spin-polarized calculations in the work were carried out based on the projector-augmented wave (PAW) method using DFT theory[2], executed with the VASP program[3]. The Perdew-Burke-Ernzerhof functional was used for exchange-correlation[4]. The effective Ueff value was set to 4eV for Mn. [5] The plane wave cutoff energy was set to 550 eV, and 3 × 3 × 1 Monkhorst-Pack k-point mesh was set for $Na_{0.5}Al_{0.5}Mn_{0.5}O_2$ 2 × 2 × 1 supercell. To calculate the electronic density of states, 5 × 5 × 3 k-point mesh for the conventional cell and the modified tetrahedron method were used. The calculated structural parameters of $Na_{0.5}Al_{0.5}Mn_{0.5}O_2$ are consistent with experimental values.

**Operando differential electrochemical mass spectrometry (DEMS)**:

Operando DEMS was utilized to study the gases generated during the cycle. The setup consisted of a commercial quadrupole mass spectrometer (Hiden HPR-20) equipped with a turbomolecular pump (Pfeiffer Vacuum) and rotary pump (Edwards Vacuum). The DEMS cell (customized Swagelok design) is integrated with two PEEK capillary tubes as with gas inlet and outlet ports. The Ar acts as the carrier with a flux of 1.0 mL/min controlled by a digital flowmeter. The DEMS cell was controlled with a LAND CT2001A battery testing system. The battery was assembled in Ar-filled glove box ($H_2O$ < 0.1 ppm, $O_2$ < 0.1 ppm), which consisted of $Na_3V_2(PO_4)_3$ (NVP) anode, 1M $NaClO_4$ in 1:1 EC/PC electrolyte, and $Na_{0.65}Al_{0.5}Mn_{0.5}O_2$ cathode. Note that $Na_3V_2(PO_4)_3$ (NVP) anode was prepared by the method reported in ref [6], and the NVP anode was half-charged before assembling the DEMS cell. In NAMO/NVP cell, anode NVP is greatly excessive with n/p≈5. The voltage of NVP vs. Na during the cycle is supposed to be constant 3.4V. The electrochemical window of the NMAO/NVP cell for the DEMS test is 3.2 V with the potentials from -2.0 V to 1.2 V.

**Table S1.** Refined parameters and atomic positions of as-prepared $Na_{1/2}Mn_{1/2}Al_{1/2}O_2$

| $Na_{0.65}Mn_{1/2}Al_{1/2}O_2$ | | | | | | |
|---|---|---|---|---|---|---|
| Space group: P 2/m Rwp=4.94% Rp=3.31% $\chi$2=4.090 a=4.9326(8)Å b=2.84499(21)Å c=5.8935(5) Å α=90° β=106.637(12)° γ=90° V=79.243(16)Å$^3$ | | | | | | |
| Atom | x/a | y/b | z/c | Multiplicity | Occupancy | 100*Uiso |
| Mn | 0.000000 | 0.000000 | 0.000000 | 1 | 1 | -0.83(8) |
| Al | 0.500000 | 0.500000 | 0.000000 | 1 | 1 | -5.05(12) |
| Na1 | 0.165(10) | 0.000000 | 0.500000 | 2 | 0.325 | 4.03(14) |
| Na2 | 0.330(10) | 0.500000 | 0.500000 | 2 | 0.325 | 4.03(14) |
| O1 | 0.3803(31) | 0.000000 | 0.1771(6) | 2 | 1 | -1.18(14) |
| O2 | 0.1771(6) | 0.500000 | 0.1771(6) | 2 | 1 | -1.18(14) |

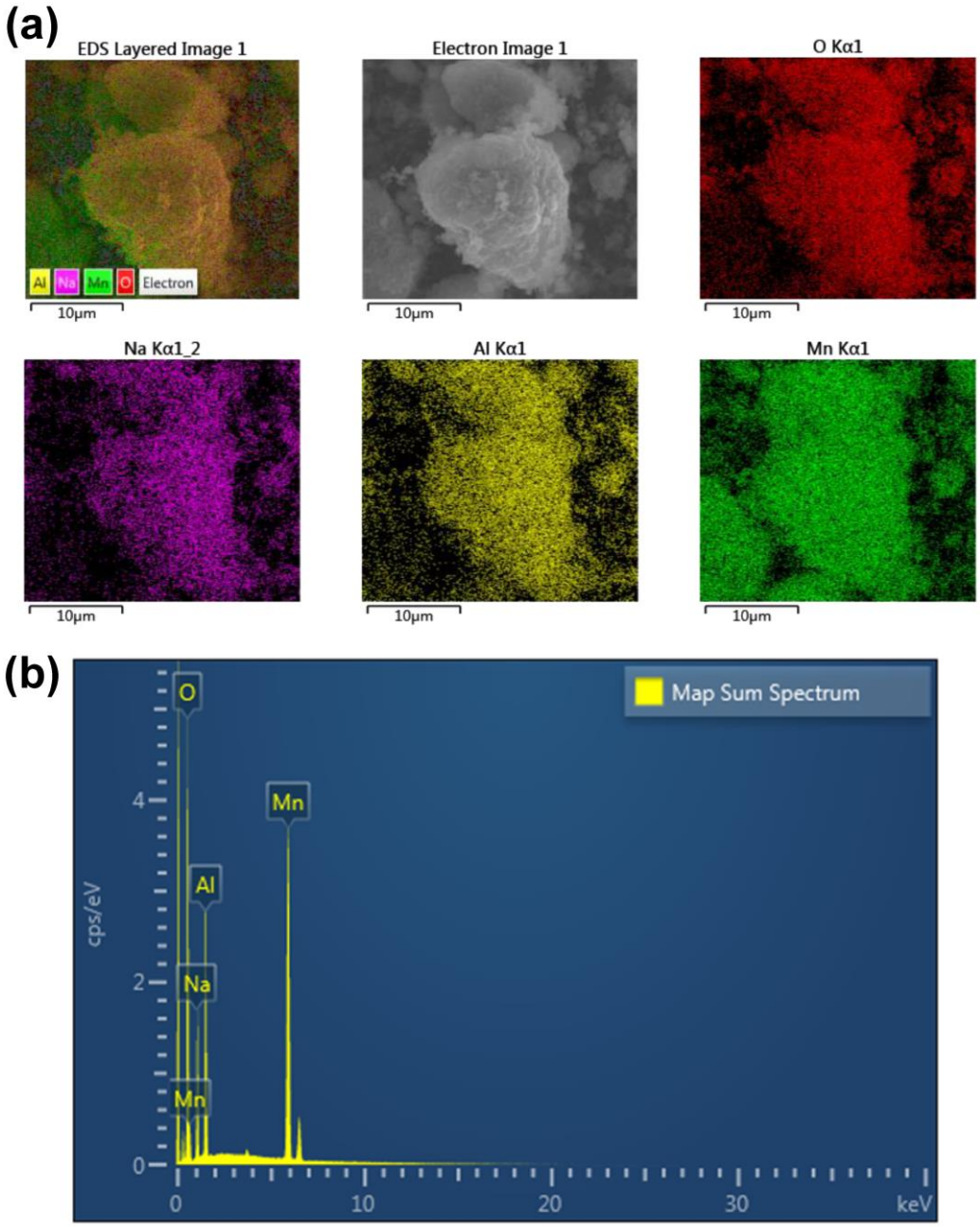


**Figure S1. (a)**EDX analysis of P3- $Na_{0.65}Al_{0.5}Mn_{0.5}O_2$ powder and corresponding elemental mapping images of O (red), Na (violet), Al (yellow), and Mn (green). **(b)**Face EDX analysis results of $Na_{0.65}Al_{1/2}Mn_{1/2}O_2$

**Table S2.** EDX element content analysis results of as-prepared $Na_{0.65}Mn_{0.5}Al_{0.5}O_2$.

| Element | Line Type | Wt% | Wt% Sigma | Standard Label | At.% Experimental | At. % Theory |
|---|---|---|---|---|---|---|
| O | K series | 40.50 | 0.23 | SiO2 | 58.31 | 54.79 |
| Na | K series | 16.73 | 0.19 | Albite | 16.76 | 17.81 |
| Al | K series | 16.07 | 0.14 | Al2O3 | 13.72 | 13.70 |
| Mn | K series | 26.71 | 0.16 | Mn | 11.21 | 13,70 |

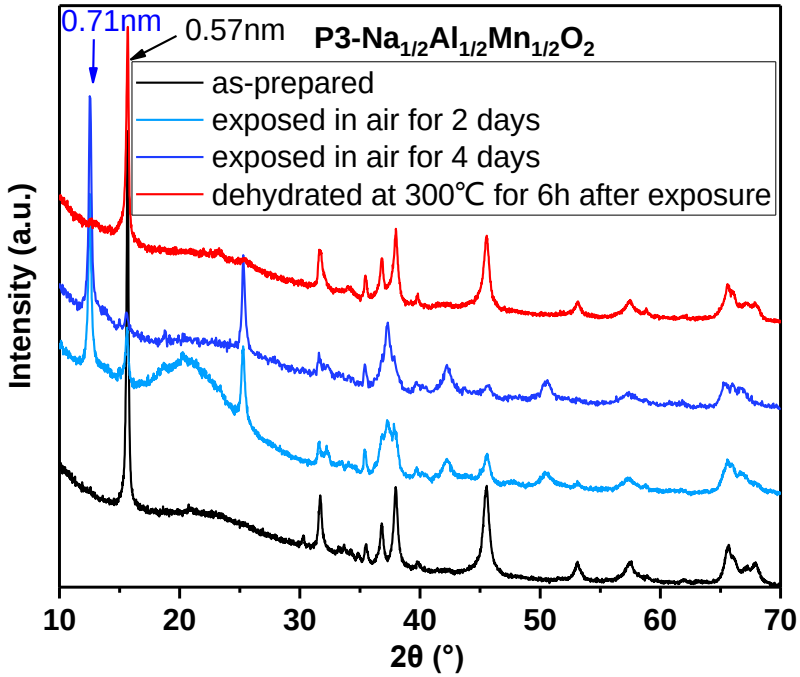


**Figure S2.** Hygroscopicity. As shown in the figure, that a new phase appeared when the as-prepared sample was exposed to air. The new phase nearly completely replaced the P3 phase after a 4-day exposure. The distance of O-TM-O slabs increase from 0.57nm to 0.71nm, which is induced by the insertion of water into the Na layer and thus transit to the birnessite structure. [7-14] The structure can recover to the origin P3 structure after being dehydrated at 300 ℃ for 6h.

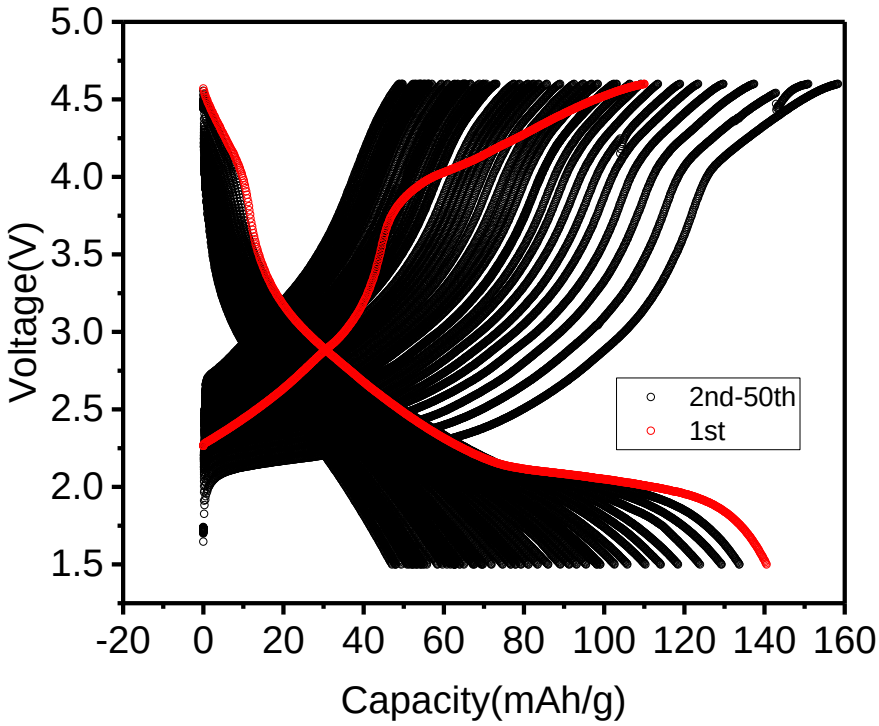


**Figure S3** Galvanostatic charge/discharge curves of $Na_{0.65}Al_{1/2}Mn_{1/2}O_2$/Na cell for 50 cycles at a rate of 10 mAh $g^{-1}$.

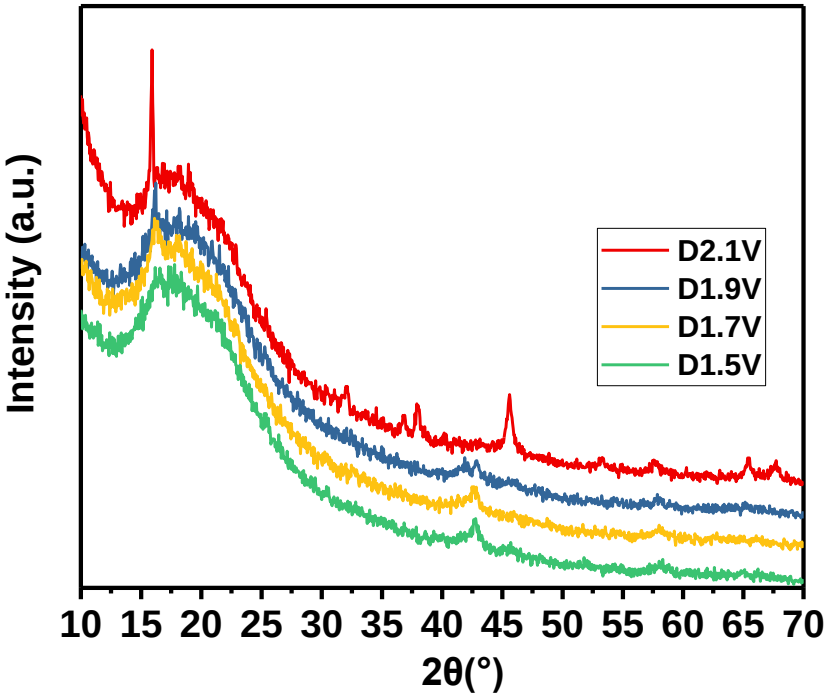


**Figure S4.** The ex-situ XRD patterns of P3-$Na_{0.65}Al_{0.5}Mn_{0.5}O_2$ electrodes for the first discharging process from 2.1V to 1.5V.

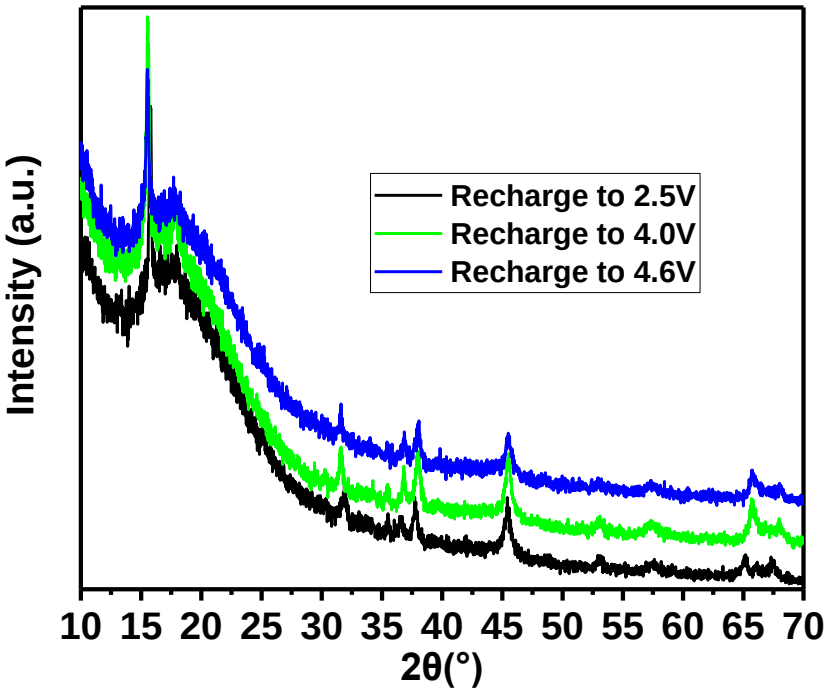


**Figure S5**. The ex-situ XRD patterns of P3-$Na_{0.65}Al_{0.5}Mn_{0.5}O_2$ electrodes for the second charging process.

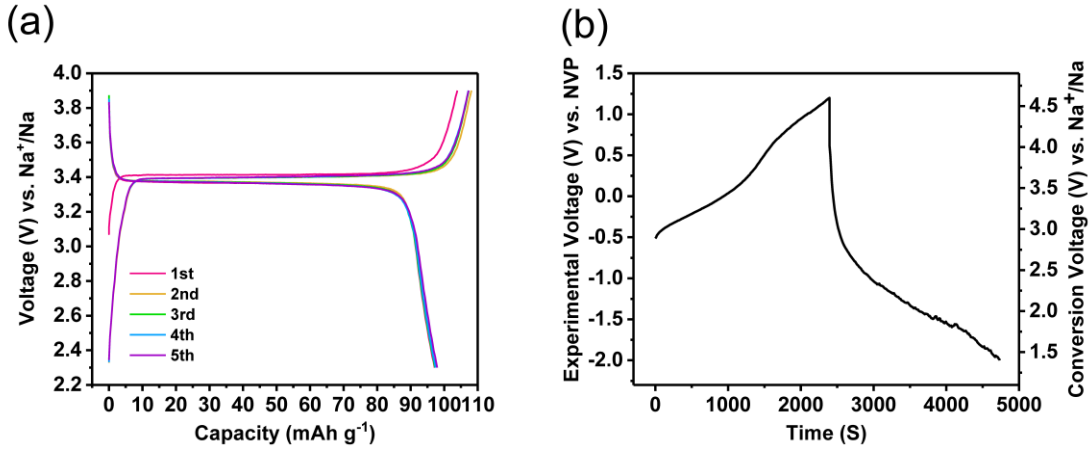


**Figure S6 (a)** Galvanostatic charge/discharge curves of NVP/Na cell at a current density of 20 mAh $g^{-1}$. The voltage of the flat plateaus of the charging and discharging process is 3.41V and 3.36V respectively, the polarization of the NVP/Na cell is ~0.05V. Besides, anode NVP is greatly excessive (N/P ≈5). The voltage of NVP vs. Na during the cycle is supposed to be constant 3.4V. **(b)** The electrochemical curve in the DEMS test. The electrochemical window of the NMAO/NVP cell for the DEMS test is -2.0V-1.2V, and the corresponding conversion electrochemical window of NMAO/Na is ~1.4V-4.6V in the DEMS experiment.

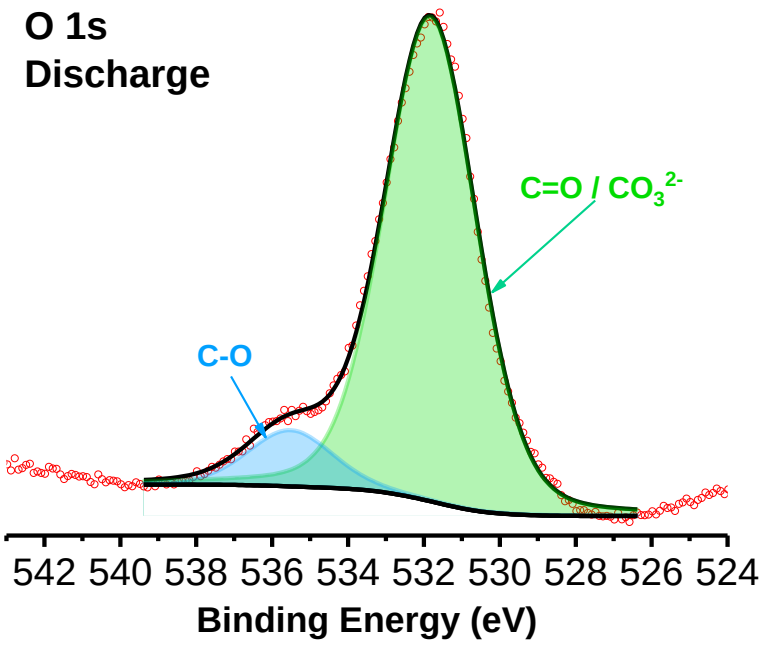


**Figure S7.** O 1s X-ray photoelectron spectroscopy (XPS) of pristine and fully-discharged $Na_{0.65}Al_{0.5}Mn_{0.5}O_2$ electrode. The lattice O can not be observed because of the solid electrolyte interface (SEI).

**Table S3.** Parameters of the peaks for XPS

| | Position (eV) | Area | FWHM (eV) |
|---|---|---|---|
| Pristine | 529.8 | 8426.7 | 1.576 |
| | 532.4 | 52543.9 | 3.261 |
| | 535.8 | 1771.1 | 1.952 |
| FC | 529.6 | 10587.3 | 1.417 |
| | 530.4 | 1460.5 | 0.911 |
| | 532.5 | 64846.4 | 3.382 |
| FD | 532.4 | 62064.4 | 2.859 |
| | 536.1 | 6612.0 | 2.631 |

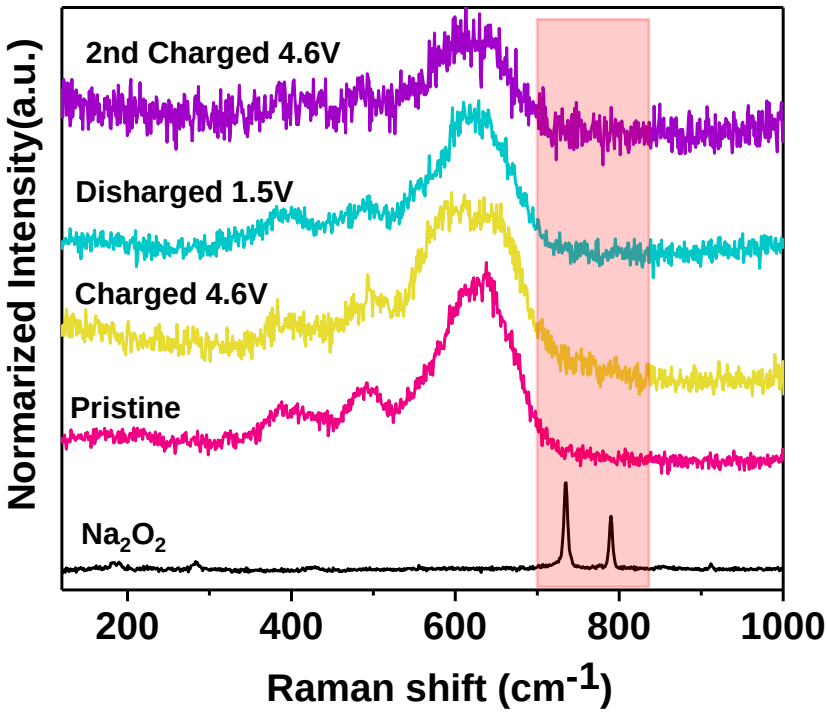


**Figure S8.** Raman spectra of $Na_{0.65}Al_{0.5}Mn_{0.5}O_2$ at different charge/discharge states. The data from $Na_2O_2$ is included for comparison.

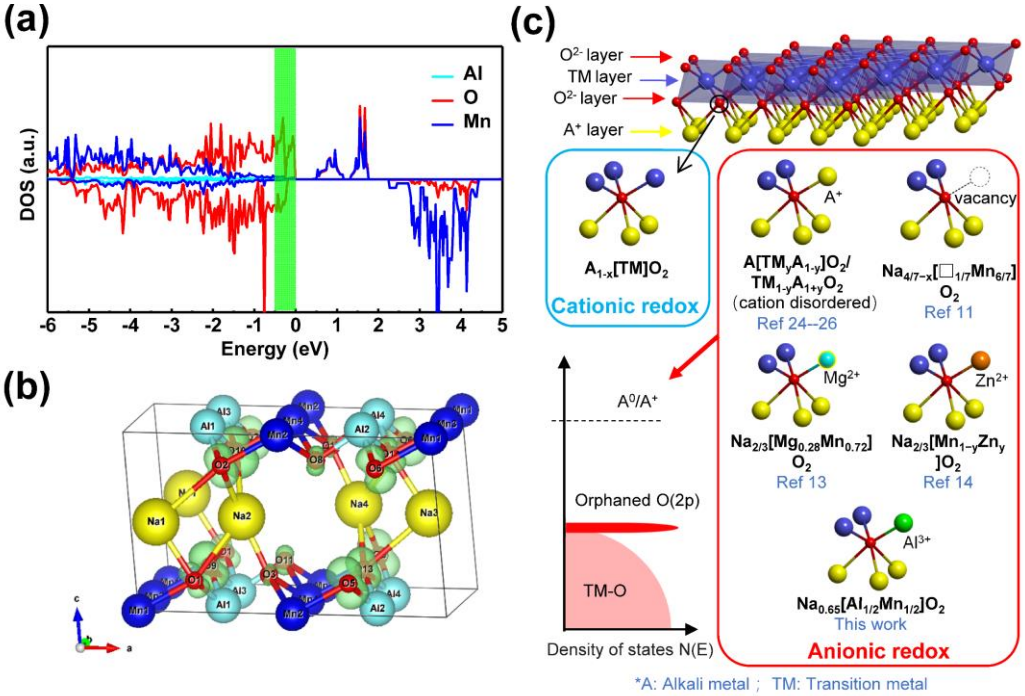


**Figure S9.** (a) The calculated density of states of $Na_{0.65}Al_{0.5}Mn_{0.5}O_2$, which is used to represent the charge contribution near the Fermi level. (b) Spatial electron density at -0.5 < E - Ef < 0 eV of $Na_{0.65}Al_{0.5}Mn_{0.5}O_2$. (c) Schematics of cationic/anionic redox.

As summarized in Figure S9c, the generally accepted mechanism of ARR was well-established in 2016, that the 2p orbitals of oxygen atoms overlap with the 2s/3s orbitals of the Li+/Na+ cations from the adjacent transition metal and alkali metal layers to form A+–O–A+ configurations, the relatively ionic nature of these interactions and relatively small overlap of O and A would create orphaned oxygen states (non-bonding states) at the top of the O-TM band to compete with transition metal-dominated complex of $e_g$* and $t_{2g}$ states and participate in charge compensation.[15-17] Layered transition metal oxides with vacancies in TM layered and affiliated orphaned oxygen states (non-bonding states) were soon revealed. In 2018, divalent $Mg^{2+}$ and $Zn^{2+}$ in TM layers were reported to trigger ARR through quasi non-bonding states generated by relative ionic M-O interaction, which exhibit peculiar properties such as no $O_2$ loss, unique ARR electrochemistry behaviour. Along with those, our work further enriches the chemistry of ARR. Trivalent $Al^{3+}$ has got no d-orbitals just as $Li^+$, $Na^+$, and $Mg^{2+}$ do, which refers to no d-O(2p) interaction. The $Al^{3+}$ 3s states are relatively high in energy compared with O 2p states, which would result in weak, ionic Al-O bonds, thus make the O 2p states relatively high in energy, which can be regarded as quasi non-bonding O orbitals, to take part in charge compensation within the stability window of the electrolyte. However, since $Li^+$/$Na^+$ and divalent $Mg^{2+}$, as well as higher electronegativity value than Li (0.98), Na (0.93), and Mg (1.31), the Al-O bond is expected to be more covalent. Trivalent $Al^{3+}$ can be an intermediate example of ionic alkali/alkaline-earth metals and high-valent (usually >3) transition metals.

## References:


1. B. Ravel and M. Newville, *J Synchrotron Radiat*, 2005, **12**, 537-541.
2. B. PE, *Phys Rev B Condens Matter*, 1994, **50**, 17953-17979.
3. G. Kresse and J. Furthmüller, *Phys Rev B Condens Matter*, 1996, **54**, 11169-11186.
4. J. P. Perdew, K. Burke and M. Ernzerhof, *Physical Review Letters*, 1998, **77**, 3865-3868.
5. S. L. Dudarev, G. A. Botton, S. Y. Savrasov, C. J. Humphreys and A. P. Sutton, *Physical Review B*, 1998, **57**, 1505-1509.
6. X. Liu, E. Wang, G. Feng, Z. Wu, W. Xiang, X. Guo, J. Li, B. Zhong and Z. Zheng, *Electrochimica Acta*, 2018, **286**, 231-241.
7. Y. Zhang, R. Zhang and Y. Huang, *Front Chem*, 2019, **7**, 335.
8. S. Boyd, R. Dhall, J. M. LeBeau and V. Augustyn, *Journal of Materials Chemistry A*, 2018, **6**, 22266-22276.
9. S. Guo, Q. Li, P. Liu, M. Chen and H. Zhou, *Nature communications*, 2017, **8**, 135.
10. K. W. Nam, S. Kim, E. Yang, Y. Jung, E. Levi, D. Aurbach and J. W. Choi, *Chemistry of Materials*, 2015, **27**, 3721-3725.
11. S. Guo, H. Yu, Z. Jian, P. Liu, Y. Zhu, X. Guo, M. Chen, M. Ishida and H. Zhou, *ChemSusChem*, 2014, **7**, 2115-2119.
12. S. Franger, S. Bach, J. P. Pereira-Ramos and N. Baffier, *Journal of the Electrochemical Society*, 2000, **147**, 3226-3230.
13. Q. Feng, H. Kanoh and K. Ooi, *Journal of Materials Chemistry*, 1999, **9**, 319-333.
14. S. Bach, J. P. Pereira-Ramos and N. Baffier, *Electrochimica Acta*, 1993, **38**, 1695-1698.
15. D. H. Seo, J. Lee, A. Urban, R. Malik, S. Kang and G. Ceder, *Nat Chem*, 2016, **8**, 692-697.
16. K. Luo, M. R. Roberts, N. Guerrini, N. Tapia-Ruiz, R. Hao, F. Massel, D. M. Pickup, S. Ramos, Y. S. Liu, J. Guo, A. V. Chadwick, L. C. Duda and P. G. Bruce, *J Am Chem Soc*, 2016, **138**, 11211-11218.
17. K. Luo, M. R. Roberts, R. Hao, N. Guerrini, D. M. Pickup, Y. S. Liu, K. Edstrom, J. Guo, A. V. Chadwick, L. C. Duda and P. G. Bruce, *Nat Chem*, 2016, **8**, 684-691.